A model of anthrax toxin lethal factor bound to protective antigen

D. Borden Lacy*, Henry C. Lin*, Roman A. Melnyk*, Ora Schueler-Furman†, Laura Reither‡, Kristina Cunningham*§, David Baker†¶, and R. John Collier*‖

*Department of Microbiology and Molecular Genetics and ‡Graduate Group of Biological Chemistry and Molecular Pharmacology, Harvard Medical School, 200 Longwood Avenue, Boston, MA 02115; and †Department of Biochemistry and ¶Howard Hughes Medical Institute, University of Washington, Seattle, WA 98195

Contributed by R. John Collier, September 21, 2005

Anthrax toxin is made up of three proteins: the edema factor (EF), lethal factor (LF) enzymes, and the multifunctional protective antigen (PA). Proteolytically activated PA heptamerizes, binds the EF/LF enzymes, and forms a pore that allows for EF/LF passage into host cells. Using directed mutagenesis, we identified three LF–PA contact points defined by a specific disulfide crosslink and two pairs of complementary charge-reversal mutations. These contact points were consistent with the lowest energy LF–PA complex found by using Rosetta protein–protein docking. These results illustrate how biochemical and computational methods can be combined to produce reliable models of large complexes. The model shows that EF and LF bind through a highly electrostatic interface, with their flexible N-terminal region positioned at the entrance of the heptameric PA pore and thus poised to initiate translocation in an N- to C-terminal direction.

computation | docking | electrostatic

Bacillus anthracis, the causative agent of anthrax, secretes three monomeric proteins, protective antigen (PA), edema factor (EF), and lethal factor (LF), that are collectively referred to as anthrax toxin (1). After its proteolytic activation and assembly into oligomeric complexes, PA can mediate the delivery of the two catalytic factors, EF and LF, into the host cell cytosol, where they can access their substrates. EF, an 89-kDa calmodulin-dependent adenylate cyclase, elevates levels of cAMP (2). LF, named for its lethal effect in animals, is a 90-kDa zinc protease that has been shown to cleave and inactivate mitogen-activated protein kinase-kinases (3, 4).

The current model for intoxication involves a multistep mechanism, the first step being binding of the 83-kDa PA monomer (PA_{83}) to a host-cell surface receptor (1). Binding is followed by proteolytic cleavage of PA_{83}, resulting in the removal of a 20-kDa fragment (PA_{20}) from the N terminus (5). The remaining 63-kDa PA (PA_{63}) is then able to oligomerize, forming a heptameric, soluble prepore (6), which, in turn, binds a maximum of three molecules of EF and/or LF (7). The limit of three has been proposed to derive from EF and LF having a footprint of binding that encompasses two PA_{63} subunits (8). The entire complex of the $(PA_{63})_7$ prepore and bound catalytic factor(s) is internalized into an endosome by receptor-mediated endocytosis (9). The increasing acidity of the endosome causes a conformational change in the prepore assembly, allowing it to penetrate the endosomal membrane and form a pore (1). This pore is thought to allow for the translocation of fully or partially unfolded EF or LF through the endosomal membrane into the cytosol, where catalysis can occur (10, 11).

EF and LF have entirely different catalytic activities but share at their N termini a common domain with significant sequence and structural homology (12, 13). This domain, referred to as EF_N or LF_N, contains the site that allows EF and LF to bind PA competitively and with high affinity ($K_d \approx 1$ nM) (14). EF_N and LF_N share a cluster of seven conserved amino acids that were shown by site-directed mutagenesis and a cell-surface binding assay to be important for binding PA (15). These residues form a relatively flat surface with dimensions of ≈10–15 Å (Fig. 1*a*). Two of the seven amino acids are Asp residues and are likely to give the binding site a net negative charge.

Binding of EF/LF depends on and potentially drives the oligomerization of PA_{63} (16). This interaction was discovered through the use of two oligomerization-deficient forms of PA, each mutated on a different PA_{63}–PA_{63} contact face. Neither form of PA alone is able to oligomerize or bind ligand, either in solution or on cells. However, when the two mutant forms of PA are combined, there is one wild-type interface that allows for dimer formation in the presence of ligand. The discovery that stable PA_{63}–PA_{63} dimers formed only in the presence of ligand led to the hypothesis that the EF/LF-binding site spanned two PA_{63} subunits. Mutations were introduced into each of the two oligomerization-deficient forms of PA to map the single ligand-binding site within dimeric PA (8). The results suggested that the EF/LF-binding site was formed by two clusters of residues separated by ≈30 Å in the PA dimer (Fig. 1*b*). The two clusters are located on a relatively flat surface and are positively charged, because combined they contain three Arg and three Lys residues.

In this study, we docked LF_N across a PA-dimer interface in two distinct orientations and evaluated these models computationally by using only their computed energies. Independently, we explored the binding by directed mutagenesis. Cys-scanning mutagenesis revealed a site where a specific disulfide crosslink can form between bound LF_N and PA, and we also found two pairs of electrostatic interactions by charge-reversal mutagenesis. The three contact points identified by the mutational analysis define a single orientation of LF_N, and this orientation coincides with the lowest energy model that emerged from the computational analysis. The binding orientation yields insights into the subsequent steps of the entry process of LF and EF, including their unfolding and translocation through the PA pore.

Materials and Methods

Modeling the Structure of the LF_N–PA Dimer Complex. To reduce computational time, the PA_{63}–PA_{63} dimer was truncated to include residues 177–260 (the subdomain that contains the EF/LF-binding site) and 458–595 (a subdomain that mediates oligomerization). The manually docked models were used as a starting point for sampling the surrounding free energy landscape by using many independent Monte Carlo minimization trajectories according to a Rosetta-Dock protocol described in refs. 17 and 18. Briefly, the rigid degrees of freedom of the starting model are randomly perturbed, and the perturbed model

Conflict of interest statement: R.J.C. holds equity in PharmAthene, Inc., a company engaged in developing countermeasures to biothreat agents, including *Bacillus anthracis*.

Abbreviations: EF, edema factor; LF, lethal factor; PA, protective antigen; rmsd, rms deviation.

§Present address: Wyeth Research, Cambridge, MA 02140.

‖To whom correspondence should be addressed. E-mail: john_collier@hms.harvard.edu.

MICROBIOLOGY

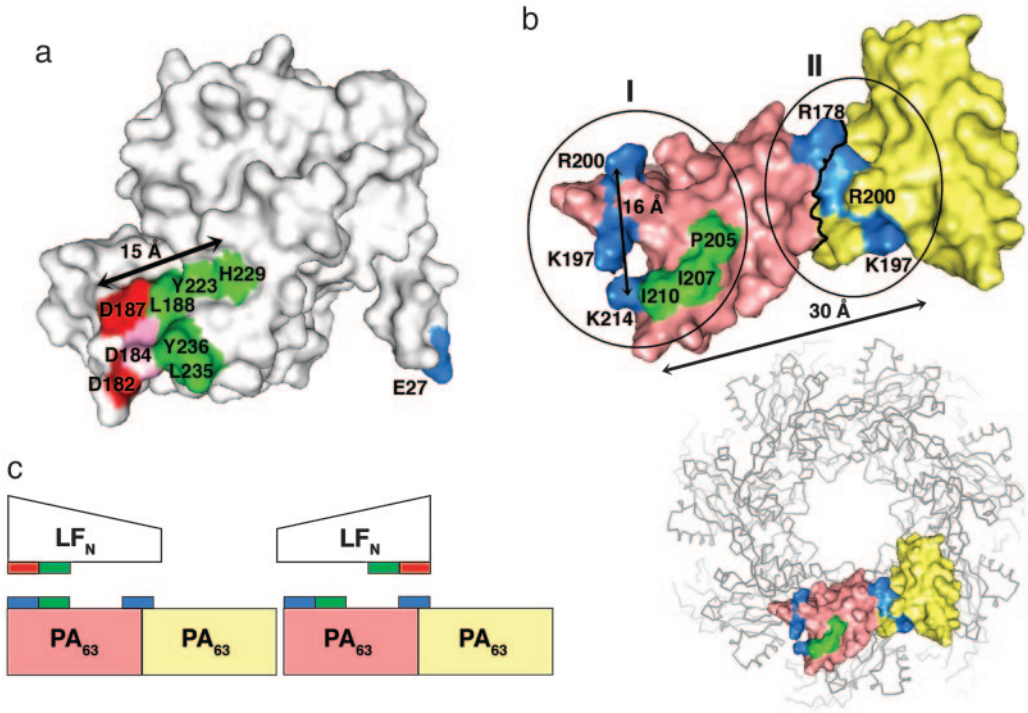

Fig. 1. Mapping the PA- and LF-binding sites by site-directed mutagenesis. (*a*) The seven residues important for binding PA (D182, D187, L188, Y223, H229, L235, and Y236) cluster on the surface of LF_N and are shown in green and red (15). (The D184A mutant did not show a binding defect but is depicted in pink, because it is likely to contribute to a net negative charge in this region.) Approximate dimensions of the site are indicated by the D187 Cα–H229 Cα distance (15 Å). The N terminus of the domain (E27) is shown in blue. (*b*) A surface rendering of the N-terminal domain 1′ (residues 175–258) from two PA_{63} subunits (yellow and pink) as viewed from the top of the heptameric ring. LF_N binding studies to dimeric PA_{63} suggested two clusters of important residues shown in green and blue (8). One cluster contains residues P205, I207, I210, K214, K197, and R200 (subsite I). The second cluster contains R178 and the K197 and R200 residues from the neighboring PA_{63} subunit (subsite II). (Note: The P205A mutant was not tested in the dimeric background but is likely part of the first subsite because of its proximity to I207. K197 and R200, which were originally tested only in the context of subsite II, have recently been shown to participate in subsite I as well; H.C.L., unpublished work.) Approximate dimensions of the site are indicated by distances of the K214 Cα to the R200 Cα of the same subunit (16 Å) and the neighboring subunit (30 Å). Coordinates for LF_N and the PA_{63}–PA_{63} dimer were obtained from the 1J7N (12) and 1TZO (25) crystal structures, respectively. (*c*) LF_N was manually docked on the PA dimer in two orientations that differed by ≈180°.

is subjected first to low-resolution refinement and then to high-resolution refinement. In the high-resolution refinement step, the side-chain and backbone degrees of freedom are optimized simultaneously in the context of a detailed all-atom energy function dominated by short-range hydrogen bonding, van der Waals interactions, and desolvation. The rms deviation (rmsd) values were calculated over the LF_N molecule after superposition of the PA dimer with the starting model.

Preparation of PA, LF_N, and Mutants. Oligonucleotides were synthesized by Integrated DNA Technologies (Coralville, IA). Mutations in PA and LF_N were made in the pET22b-PA (1–735) (19) and pET15b-LF_N (1–263) (15) constructs, respectively, by using the QuikChange method (Stratagene) of site-directed mutagenesis. ^{35}S-labeled LF_N proteins were produced by *in vitro* transcription/translation by using a TNT coupled reticulocyte lysate system (Promega). Otherwise, PA and LF_N were expressed and purified from *Escherichia coli* as described in refs. 20 and 21. PA was activated by using a trypsin-to-PA ratio of 1:1,000 (wt/wt). The mixture was incubated at room temperature for 30 min and quenched with a 10 M excess of soybean trypsin inhibitor.

Disulfide Crosslinking. Activated PA was incubated with an equimolar amount of LF_N in the presence of excess DTT for 1 h on ice to allow for binding. The PA–LF_N mixture was applied to a Sephadex G-25 column (Amersham Pharmacia) to remove DTT and exchange the complex into a buffer containing 50 mM NaCl and 20 mM Tris·Cl (pH 8.0). Samples were allowed to oxidize for 10 min before adding *N*-ethylmaleimide to quench any remaining free cysteines. The proteins were precipitated with trichloroacetic acid, resuspended in SDS buffer, and then analyzed by SDS/PAGE using a 7.5% acrylamide/SDS gel. Gels were stained with Coomassie blue.

Binding Assay for Charge-Reversal Mutations. PA-mediated binding of ^{35}S-labeled LF_N was performed on CHO-K1 cells (CCL-61, American Type Culture Collection) as described in ref. 22. Supplies for cell culture media were from Invitrogen. Cells were grown in Ham's F-12 medium supplemented with 10% calf serum, 500 units/ml penicillin G, and 500 units/ml streptomycin sulfate and were maintained as monolayers in a humidified atmosphere of 5% CO_2. The cells (2×10^5 cells per well) were incubated on ice with 2.4×10^{-8} M trypsin-nicked PA for 1 h. The cells were washed with PBS and incubated on ice with ^{35}S-labeled LF_N for 1 h. Cells were washed three times with PBS and treated with lysis buffer, and the radioactive content was determined by scintillation counting.

Results

Creating a Model of LF_N Bound to a PA Dimer. LF_N was manually docked on a truncated PA dimer in two orientations that differed by ≈180° (Fig. 1*c*). In the first orientation (Fig. 1*c Left*), the PA-binding site on LF_N was aligned to subsite I of PA to maximize both the charge complementarity between the negatively and positively charged amino acids and the overlap of

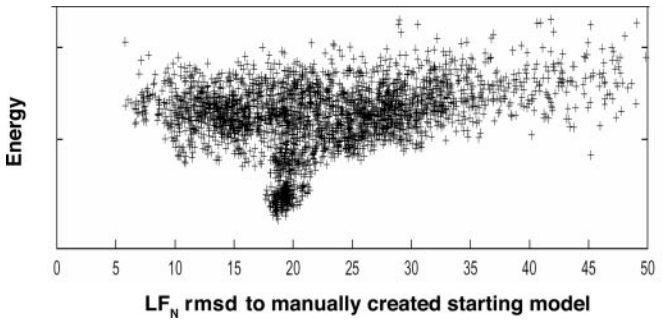

Fig. 2. The Rosetta-Dock model of the LF_N–PA dimer complex lies in a deep energy funnel. Three thousand independent trajectories were carried out, starting from the manually docked model. The energy for each structure (arbitrary units) is plotted against the rmsd between LF_N molecules when the PA subunits from the manually docked and final models are aligned. There is a dramatic energy funnel around 20 Å from the starting model. The lowest energy structure also is the center of the largest cluster of low-energy models, and it is our most reliable model for this complex.

hydrophobic residues. In the second orientation (Fig. 1*c Right*), the negatively charged residues of the LF_N PA-binding site were aligned to PA subsite II. Both models were then subjected to refinement by using the Rosetta-Dock protocol. To sample the free-energy landscape in the vicinity of the manually docked models, we carried out 3,000 independent refinement trajectories starting from random perturbations of the starting models (see *Materials and Methods*). Whereas the refinement of models from the second orientation did not result in an energetic minimum (data not shown), the energy landscape produced by the refinement from the first orientation (Fig. 2) contained a pronounced energy minimum. Alignment of the PA dimers indicates that, in these low-energy models, LF_N differs from the starting model by ≈20 Å rmsd. Dramatic energy funnels, such as this one, were found post facto to be strong indicators of the correctness of a prediction in the double-blind Critical Assessment of Predicted Interactions (CAPRI) protein–protein docking experiment in which a number of the predictions made by using the Rosetta-Dock protocol turned out to have close to atomic-level accuracy (18, 23). We chose the lowest energy model generated, the lowest energy point in Fig. 2, as our prediction. It should be emphasized that the model was selected based on energy criteria alone, and that no experimental information was used other than that implicit in the manually docked starting structures.

Identification of a Disulfide Crosslink Between LF_N Y108C and PA N209C. Because neither LF nor PA contains cysteine, introducing cysteines by site-directed mutagenesis represents a straightforward method to test for formation of disulfide crosslinks with binding. First, heptameric, wild-type PA_{63} or PA_{63} N209C was incubated with wild-type LF_N or one of seven LF_N mutants: Y108C, K110C, Y118C, Q132C, S134C, D136C, and Q228C. Binding was allowed to occur in the presence of excess DTT to prevent the formation of nonspecific disulfides. The DTT was then removed, and the samples were allowed to oxidize briefly before being treated with *N*-ethylmaleimide. The formation of a disulfide crosslink between LF_N Y108C and PA_{63} N209C was visible as a slow-mobility band on an SDS gel that could be disrupted in the presence of DTT (Fig. 3). This band was shown by Western blotting with anti-PA and anti-LF_N antibodies to contain both PA and LF_N (data not shown). The crosslink formed selectively, because LF_N K110C, Y118C, Q132C, S134C, D136D, and Q228C did not form crosslinks when incubated with PA_{63} N209C (data not shown). Likewise, LF_N Y108C did not crosslink with PA_{63} S186C (data not shown).

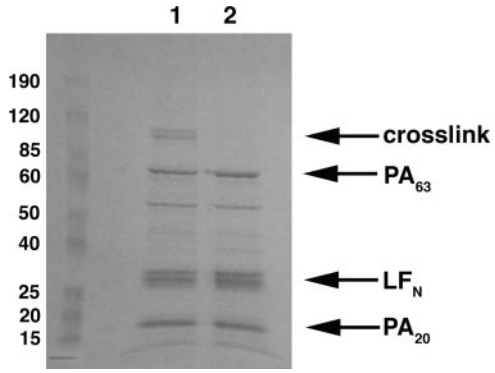

Fig. 3. Identification of a disulfide crosslink between LF_N Y108C and PA N209C. LF_N Y108C and PA_{63} N209C form a disulfide-linked complex under oxidizing conditions (lane 1), which is disrupted in the presence of 10 mM DTT (lane 2).

Identification of Complementary Charge-Reversal Mutations That Can Rescue Binding. The LF_N- and PA-binding surfaces are notable in that they contain a large number of negatively and positively charged residues, respectively. The idea that electrostatics might play an important role in the binding interaction suggested that it might be possible to exchange a specific negative residue in LF_N and a positive residue in PA in a way that would not compromise the binding interaction.

Reversing the charge in six of the positively charged residues of PA (R178D, K197D, R200E, K213E, K214E, and K218E) inhibited binding of wild-type LF_N, (binding was observed at 0–63% of wild-type levels, Fig. 4). Similarly, substituting a lysine for LF_N D187 reduced PA-binding to 3% of wild-type levels. Pairing the LF_N D187K mutant with each of the six PA charge-reversal mutants restored binding to 120% of wild-type levels in the case of the LF_N D187K–PA K213E pair but had no significant effect on the other five PA mutants (Fig. 4). After identifying the LF_N D187K–PA K213E pair, LF_N D187K also

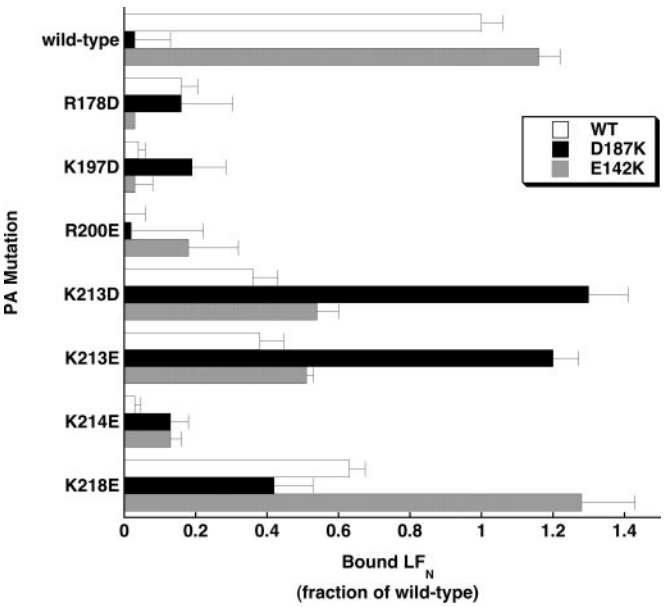

Fig. 4. A cell-surface binding assay shows that the LF_N D187K–PA K213D/K213E and LF_N E142K–PA K218E pairs can rescue binding defects. Data represent the fraction of mutant ^{35}S-labeled LF_N bound specifically to PA on cells relative to that of wild-type LF_N. Error bars represent SEM.

MICROBIOLOGY

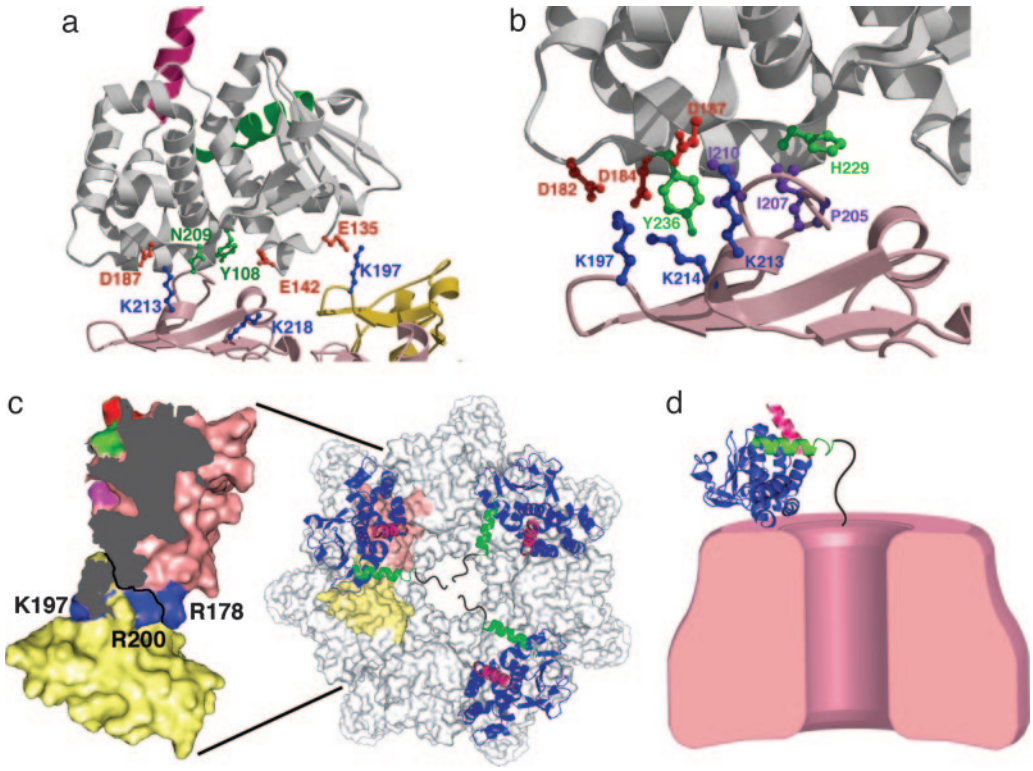

Fig. 5. The model of LF_N bound to PA. (*a*) In this depiction of LF_N (gray) bound to the surface of dimeric PA_{63} (light pink and yellow), the LF_N E135, E142, and D187 residues are shown in red; the PA K197, K213 and K218 residues are shown in blue; and the LF_N Y108–PA N209 pair from the disulfide crosslinking experiment is shown in green. (Note: The E135 and K197 residues are predicted to interact based on the model but were not able to complement each other in a charge-reversal experiment.) As modeled, the bulk of LF_N's contacts are with a single PA_{63} subunit (light pink), but contacts do exist with the neighboring PA_{63} subunit (yellow). The N- and C-terminal helices of LF_N are shown in green and bright pink, respectively. (*b*) A close-up of the modeled interface between LF_N and PA subsite I suggests a large number of electrostatic interactions and a buried LF_N His residue. Residues from LF_N and PA that may form electrostatic interactions are shown in red and blue, respectively. LF_N H229 and Y236 were identified as the two most important residues for binding PA (15) and are shown in green, whereas the three important hydrophobic residues from the PA ligand-binding site (8) are shown in purple. (*c*) An aerial view of the PA heptamer–LF_N complex in which three LF_N molecules are bound. The footprint for LF_N contacts on the PA dimer is shown in gray. LF_N does not make contacts with residues R178 and R200 at subsite II. The three experimentally obtained PA contact points (K213, N209, and K218) are shown in red, green, and purple, respectively. The N- and C-terminal helices of LF_N are shown in green and bright pink, respectively. (*d*) A cartoon side view of the LF_N–PA complex in which only one LF_N (blue) is bound. PA is depicted as a cartoon cutaway to emphasize the interior lumen of the heptameric ring. As modeled, the N-terminal helix of LF_N (green) points toward the interior of the heptameric ring, whereas the C-terminal helix (bright pink) points upward and away from the heptamer, thereby allowing room for the LF catalytic domain. The N-terminal 26 residues of LF_N are drawn in cartoon format as a black line and can potentially insert into the prepore lumen. LF translocation is thought to be initiated by the LF N terminus and occur through the lumen of the heptameric ring (11, 24).

was tested against PA K213D and shown to restore binding to 130% of wild-type levels (Fig. 4).

A similar experiment was conducted in which a LF_N E142K mutant was paired against the seven PA charge-reversal mutants. Although the LF_N E142K mutant on its own was not defective in binding wild-type PA (it binds at 116% of the wild-type level), the mutation rescued the binding defect in K218E, such that binding for the pair was at 128% that of wild-type (Fig. 4). E142K failed to complement the binding defects in the other six PA mutants tested.

Discussion

The goal for this study was to generate a model for how LF_N binds to and is oriented on PA. Simple docking was initially confounded by the large discrepancy in size of the two putative binding sites (Fig. 1 *a* and *b*). To circumvent this problem, we adopted three approaches to further explore this molecular interface.

The first was to model the complex in two extremely different orientations and then select a model based solely on their energies. The flat, rectangular shape of the surfaces containing the LF_N- and PA-binding sites, along with the clusters of negatively and positively charged residues within these binding sites, suggested that, to a first approximation, LF_N would bind the PA dimer in one of two orientations (Fig. 1*c*). We docked LF_N to a PA dimer in orientations that differed by ≈180° and submitted both models to energetic minimization using a Rosetta-Dock protocol. We observed a dramatic energy funnel for the model in which the PA-binding site of LF_N was docked to PA subsite I (Fig. 2).

The second approach was to identify one or more points where a disulfide crosslink could be effected between LF_N and PA. We chose residues in LF_N and PA that were located near the binding sites but where alanine substitution had been shown not to affect binding (8, 15). We introduced cysteine mutations in these positions and observed a specific disulfide crosslink between LF_N Y108C and PA N209C (Fig. 3). In the energetically favorable model, the distance between LF_N Y108 and PA N209 is consistent with a disulfide being able to form if cysteines were substituted at these positions (Fig. 5*a*).

The final approach was designed to identify pairs of charged residues in the two proteins that could be reversed without inhibiting the interaction; this approach also was expected to yield insights into the importance of electrostatics in the LF_N–PA interaction. We found that reversing the charge of certain residues in LF_N or PA could inhibit binding to the wild-type

partner protein and reasoned that pairing these charge-reversal mutants so that they could maintain an electrostatic interaction might rescue binding for these otherwise defective mutants. We identified two such pairs of charge-reversal mutants: LF_N D187K–PA K213D/K213E and LF_N E142K–PA K218E, suggesting that the LF_N D187–PA K213 and LF_N E142–PA K218 residues are close in the LF_N–PA complex (Fig. 4). In the low-energy model, the charge pairs are located on either side of the disulfide crosslink (Fig. 5*a*). Although the Rosetta-Dock protocol does not emphasize electrostatics, the model suggests that, with modest rearrangement of side chain rotamers, these pairs of residues should be close enough to form favorable electrostatic interactions.

Alignment of the PA molecules from the energetically favorable model and its starting model reveals that LF_N has shifted by a rmsd of 20 Å. This large departure from the starting model is because of a twist in LF_N that unexpectedly minimizes the interaction of LF_N with PA subsite II. As modeled, LF_N contacts the K197 residue of the PA_{63}–PA_{63} interface but does not make any direct contacts with R178 and R200 (the two other residues of the second subsite suggested by the mutagenesis work done in the PA dimer; ref. 8) (Figs. 1*b* and 5*c*). We found that it was not possible to identify an alternate low-energy model in which LF_N could interact with these residues. One possibility is that there is a conformational change in LF_N and/or PA that could not be modeled by using rigid backbone structures. We now question, however, whether LF_N-dependent dimerization of the oligomerization-deficient PA mutants yielded an unambiguous map of binding defects. Because R178, K197, and R200 are located at the dimer interface, it is possible that mutation of these residues causes oligomerization defects and does not directly affect ligand binding. Because PA dimers are formed only in the presence of ligand, it is difficult to distinguish these two possibilities. Given that the subsite II data may not reflect LF_N binding and that the model recapitulates the independently identified disulfide and electrostatic pairs, we propose the low-energy model as a reliable prediction of the LF_N–PA dimer complex structure. The fact that a purely energy-based prediction can reproduce the experimental results quite well and even point at possible incorrect information is encouraging and demonstrates that high-resolution structure prediction can make useful contributions to the structural characterization of a protein–protein interface, particularly in conjunction with experimental data. The combination of experimental and computational methods in this study may represent the beginning of a new paradigm for structure determination as computational methods become more accurate and structural biologists seek to understand larger and more complex systems that are less amenable to traditional high-resolution structure-determination methods.

The energetically favorable model has LF_N spanning two neighboring PA_{63} subunits with a buried surface area of 2,300 $Å^2$ (Fig. 5 *a* and *c*). Although no experiments were conducted on the EF_N–PA interaction for this study, the EF_N structure aligns to the LF_N of the refined model with an rmsd of 1.7 $Å^2$ for 191 Cα atoms, suggesting that EF_N and LF_N bind PA similarly. By contrast, the LF_N-binding site overlaps but is distinct from the PA_{20}-binding sites. PA cannot oligomerize in the presence of PA_{20} because of steric clash. The model shows that a single LF_N molecule binds across two neighboring PA_{63} subunits and displaces the PA_{20} fragments of both subunits. This may explain why ligand binding is so important for PA oligomerization.

The bulk of the LF_N interactions are nonetheless with a single PA_{63} subunit. There is excellent packing between the PA-binding site on LF_N (Fig. 1*a*) and the PA ligand-binding subsite I (Fig. 1*b*) with a significant number of electrostatic interactions (Fig. 5*b*). The interface also contains a buried His residue contributed by LF_N, H229. The prevalence of charged residues at the interface may be relevant to the pH dependence of the subsequent steps of translocation. The low pH of the endosome triggers conversion of the PA heptameric prepore to the pore and initiates the process of ligand translocation. Low pH also seems to aid the unfolding of LF_N, a process required to transport such a large molecule through the narrow pore lumen (10). Because the enzymatic ligand ultimately needs to be released from the heptamer surface to be translocated, there may be a pH dependence to the binding affinity as well. This pH dependence could be achieved by having a high number of charged and/or titratable residues at the interface.

An electrostatic interaction also may be involved in LF_N's contacts with the PA_{63}–PA_{63} interface, because the model indicates that LF_N E135 and the K197 residue from the neighboring PA subunit will be in close proximity (Fig. 5*a*). An attempt to verify this interaction by pairing charge-reversal mutants was unsuccessful (data not shown) but may reflect the fact that PA K197 contributes to the binding interaction from both subunits (Fig. 1*b*). Despite the lack of direct contacts with R178 and R200 of subsite II, the model does suggest that LF_N spans an interface and structurally occludes the neighboring subunit of PA (Fig. 5*c*). This occlusion is consistent with the observations that only three molecules of $EF/LF/LF_N$ can bind the heptamer at one time (7) and that the PA_{63} dimer formed from two nonoligomerizing mutants binds only a single LF_N molecule (16). Finally, the model indicates that the N-terminal α-helix of LF_N is oriented over the luminal space of the PA heptamer (Fig. 5 *c* and *d*). This helix, corresponding to residues 27–43, represents the first visible part of the LF_N crystal structure, because the N-terminal 26 residues are presumably disordered (12). It has been shown that the N terminus initiates the translocation of LF_N through the lumen of the PA heptameric pore (24). Having LF_N bound such that the N-terminal helix is poised above this opening should facilitate this process and may mean that the N-terminal 26 residues can bind inside the prepore lumen before the beginning of pore formation and translocation (Fig. 5*d*).

This work was supported by a Charles A. King Trust postdoctoral fellowship (to D.B.L.) and National Institutes of Health Grant AI022021.

1. Collier, R. J. & Young, J. A. (2003) *Annu. Rev. Cell Dev. Biol.* **19,** 45–70.
2. Leppla, S. H. (1982) *Proc. Natl. Acad. Sci. USA* **79,** 3162–3166.
3. Duesbery, N. S., Webb, C. P., Leppla, S. H., Gordon, V. M., Klimpel, K. R., Copeland, T. D., Ahn, N. G., Oskarsson, M. K., Fukasawa, K., Paull, K. D. & Vande Woude, G. F. (1998) *Science* **280,** 734–737.
4. Vitale, G., Pellizzari, R., Recchi, C., Napolitani, G., Mock, M. & Montecucco, C. (1998) *Biochem. Biophys. Res. Commun.* **248,** 706–711.
5. Molloy, S. S., Bresnahan, P. A., Leppla, S. H., Klimpel, K. R. & Thomas, G. (1992) *J. Biol. Chem.* **267,** 16396–16402.
6. Milne, J. C., Furlong, D., Hanna, P. C., Wall, J. S. & Collier, R. J. (1994) *J. Biol. Chem.* **269,** 20607–20612.
7. Mogridge, J., Cunningham, K. & Collier, R. J. (2002) *Biochemistry* **41,** 1079–1082.
8. Cunningham, K., Lacy, D. B., Mogridge, J. & Collier, R. J. (2002) *Proc. Natl. Acad. Sci. USA* **99,** 7049–7053.
9. Gordon, V. M., Leppla, S. H. & Hewlett, E. L. (1988) *Infect. Immun.* **56,** 1066–1069.
10. Krantz, B. A., Trivedi, A. D., Cunningham, K., Christensen, K. A. & Collier, R. J. (2004) *J. Mol. Biol.* **344,** 739–756.
11. Zhang, S., Udho, E., Wu, Z., Collier, R. J. & Finkelstein, A. (2004) *Biophys. J.* **87,** 3842–3849.
12. Pannifer, A. D., Wong, T. Y., Schwarzenbacher, R., Renatus, M., Petosa, C., Bienkowska, J., Lacy, D. B., Collier, R. J., Park, S., Leppla, S. H., *et al.* (2001) *Nature* **414,** 229–233.
13. Shen, Y., Zhukovskaya, N. L., Guo, Q., Florian, J. & Tang, W. J. (2005) *EMBO J.* **24,** 929–941.
14. Elliott, J. L., Mogridge, J. & Collier, R. J. (2000) *Biochemistry* **39,** 6706–6713.
15. Lacy, D. B., Mourez, M., Fouassier, A. & Collier, R. J. (2002) *J. Biol. Chem.* **277,** 3006–3010.

16. Mogridge, J., Cunningham, K., Lacy, D. B., Mourez, M. & Collier, R. J. (2002) *Proc. Natl. Acad. Sci. USA* **99,** 7045–7048.
17. Gray, J. J., Moughon, S., Wang, C., Schueler-Furman, O., Kuhlman, B., Rohl, C. A. & Baker, D. (2003) *J. Mol. Biol.* **331,** 281–299.
18. Schueler-Furman, O., Wang, C. & Baker, D. (2005) *Proteins* **60,** 187–194.
19. Benson, E. L., Huynh, P. D., Finkelstein, A. & Collier, R. J. (1998) *Biochemistry* **37,** 3941–3948.
20. Wigelsworth, D. J., Krantz, B. A., Christensen, K. A., Lacy, D. B., Juris, S. J. & Collier, R. J. (2004) *J. Biol. Chem.* **279,** 23349–23356.
21. Zhao, J., Milne, J. C. & Collier, R. J. (1995) *J. Biol. Chem.* **270,** 18626–18630.
22. Wesche, J., Elliott, J. L., Falnes, P. O., Olsnes, S. & Collier, R. J. (1998) *Biochemistry* **37,** 15737–15746.
23. Schueler-Furman, O., Wang, C., Bradley, P., Misura, K. & Baker, D., *Science*, in press.
24. Zhang, S., Finkelstein, A. & Collier, R. J. (2004) *Proc. Natl. Acad. Sci. USA* **101,** 16756–16761.
25. Lacy, D. B., Wigelsworth, D. J., Melnyk, R. A., Harrison, S. C. & Collier, R. J. (2004) *Proc. Natl. Acad. Sci. USA* **101,** 13147–13151.